Ore Geology Reviews 105 (2019) 605–615

Contents lists available at ScienceDirect

Ore Geology Reviews

journal homepage: www.elsevier.com/locate/oregeorev

Mantle-derived and crustal He and Ar in the ore-forming fluids of the Xihuashan granite-associated tungsten ore deposit, South China

Wen-Feng Wei[a,b], Rui-Zhong Hu[b,c,*], Xian-Wu Bi[b], Guo-Hao Jiang[b], Bing Yan[a], Run-Sheng Yin[b], Jie-Hua Yang[b]

[a] Institute of Earth Sciences, Chengdu University of Technology, Chengdu 610059, China
[b] State Key Laboratory of Ore Deposit Geochemistry, Institute of Geochemistry, Chinese Academy of Sciences, Guiyang 550081, China
[c] University of Chinese Academy of Sciences, Beijing 100039, China

ARTICLE INFO

Keywords:
Xihuashan tungsten deposit
He and Ar isotopes
Ore-forming fluids
Crust-mantle interaction
South China

ABSTRACT

The Xihuashan tungsten ore deposit in the central Nanling region, South China is a vein-type hydrothermal deposit associated with the Late Jurassic granitoids that were previously thought to be the products of crustal anatexis alone. In this study, we use helium (He) and argon (Ar) isotopes of fluid inclusions entrapped in pyrite and arsenopyrite to determine the origin of the ore-forming fluids. The $^{3}He/^{4}He$ ratios of the crushed fluid inclusions vary from 0.15 to 1.16 Ra, with a mean of 0.72 Ra (Ra, the atmospheric $^{3}He/^{4}He$ ratio of 1.4×10^{-6}), indicating the presence of mantle-derived noble gasses in the fluids. The amounts of the mantle-derived noble gasses are estimated to be between ~2 and 17%. The $^{40}Ar/^{36}Ar$ ratios of the fluid inclusions vary from 306 to 1023, with an average of 440. These ratios are significantly higher than the average crustal value, indicating the presence of air-saturated water in the volatiles released from the mineral separates. The results from this study indicate that the associated, coeval granitoids, which is believed to provide the ore-forming fluids during magma evolution, are not the products of pure crustal melts. Mantle-derived volatiles and heat was also involved in the genesis of the host granite pluton.

1. Introduction

W-Sn polymetallic deposits are widespread in the Nanling region, South China. In the past ten years the Jiangnan Tungsten Belt (JTB), comprising several super-large W polymetallic deposits, located north to the Nanling W-Sn region, has been newly defined. Both the Nanling region and JTB are the important regions for further exploration of world-class W ore deposits (Mao et al., 2015, 2017; Wei et al., 2017, 2008). In the Nanling region most of W deposits are spatially, temporally and genetically associated with Jurassic S-type granitoids, which are previously believed to be produced by crustal anatexis, without any mantle contribution (Wu et al., 1987; Chen et al., 2008a; Wang, 2008). Recently, a growing number of studies show that mantle-derived magmas were involved in the genesis of some W deposits and associated granitoids in the region based on isotope data and whole rock compositions (e.g., Lu, 1986; Liu et al., 2002; Hsieh et al., 2008; Yang et al., 2012; Li et al., 2016). However, due to composition convergence and/or hydrothermal alteration, these data are not decisive constraints on the involvement of mantle component in the genesis of the W deposits and associated granitoids (Li et al., 2009).

Noble gas isotopes, especially Helium and argon isotopes are more useful for identifying the presence of mantle component in magma and hydrothermal fluids (e.g., Stuart et al., 1995; Hu et al., 1998a; Burnard et al., 1999; Ballentine and Burnard, 2002). ^{3}He and ^{36}Ar are concentrated in the mantle and atmosphere, respectively (e.g., Bouabdellah et al., 2015). ^{4}He and ^{40}Ar are produced by radioactive decay dominantly in the crust (e.g., Landis and Hofstra, 2012). The isotope ratios of helium and argon are generally more meaningful than their abundance ratios because the former can provide definitive information on source(s) (Kendrick and Burnard, 2013). Because of the distinctive isotope ratios in different geochemical reservoirs, $^{3}He/^{4}He$ values can provide clear evidence for the involvement of mantle-derived volatiles, and $^{40}Ar/^{36}Ar$ variations can provide additional constraints on the fluid source(s) in various ore deposit types (e.g., Stuart et al., 1995; Hu et al., 1998a, 1998b, 1999, 2004, 2009, 2012a; Burnard and Polya, 2004; Li et al., 2007; Kendrick et al., 2007; Wu et al., 2011; Marschik and Kendrick, 2015). For example, the $^{3}He/^{4}He$ ratios (0.1–3.03 Ra) of fluid inclusions in sulfides from most Asian W deposits point to the involvement of mantle-derived fluids, possibly magmatic hydrothermal fluids (Dae-Hwa, Korean; Stuart et al., 1995; Yaogangxian, China; Hu

* Corresponding author at: State Key Laboratory of Ore Deposit Geochemistry, Institute of Geochemistry, Chinese Academy of Sciences, Guiyang 550081, China.
E-mail address: huruizhong@vip.gyig.ac.cn (R.-Z. Hu).

https://doi.org/10.1016/j.oregeorev.2019.01.014
Received 4 January 2017; Received in revised form 1 August 2018; Accepted 16 January 2019
Available online 17 January 2019
0169-1368/

et al., 2012a). The $^{40}Ar/^{36}Ar$ ratios of the ore-forming fluids are also variable, ranging from as high as ~2952 coupled with high $^{3}He/^{4}He$ of 4.36 Ra (Zhai et al., 2012) to low values of 255–800 that can be attributed to the involvement of atmospheric components (the atmospheric $^{40}Ar/^{36}Ar$ ratio is 295.5, Stuart et al., 1995) according to the majority of studies (e.g., Burnard et al., 1999; Burnard and Polya, 2004; Wu et al., 2011; Hu et al., 2012a; Moura et al., 2014).

The Xihuashan W ore deposit, discovered more than a century ago, is one of the largest in the world (Guo et al., 2012). Local geologist reported that the accumulate reserve in the Xihuashan is more than 120,000 tonnes of WO_3. Most of the studies on the Xihuashan deposit were conducted in the last few decades. Previous studies mainly focused on the geology, geochemistry, fluid inclusions and geochronology of W mineralization (e.g., Wu et al., 1987; Giuliani et al., 1988; Shen et al., 1994; Zeng et al., 2001; Guo et al., 2012; Hu et al., 2012b; Wei et al., 2012). The previous studies suggested that the associated Late Jurassic granite provided additional hydrothermal fluids to the ore-forming fluids of the deposit (e.g., Hu and Zhou, 2012; Wei et al., 2012). However, it remains unclear how and to what extent mantle components were added. In this study, He-Ar isotope data of fluid inclusions in pyrite and arsenopyrite in the deposit are used to improve our understanding on the sources of ore-forming fluids.

2. Geological background

2.1. Regional geology

South China comprises the Yangtze and Cathaysia Blocks, which collided at ca. 830 Ma along the Jiangshan-Shaoxing suture (Fig. 1a, b) (Zhou et al., 2002, 2006; Yan et al., 2003; Zhao et al., 2011; Yuan et al., 2012, 2015, 2018a; Zhong et al., 2017; Zhao et al., 2018). The Cathaysia Block is characterized by widespread Mesozoic granitic magmatism and associated metallogeny, such as W, Sn, and U mineralisation (e.g., Zhao et al., 2016; Xie et al., 2018a,b; Yuan et al., 2018b). In the Cathaysia Block, the Archean basement is overlain by Mesoproterozoic-Ordovician flysch sequences, which are unconformably overlain by Devonian to Triassic sedimentary rocks and intruded by widespread Mesozoic igneous rocks (Gilder et al., 1996; Chen and Jahn, 1998; Hsieh et al., 2008; Liu et al., 2014). The Cathaysia Block can be further subdivided into northwestern and southeastern Cathaysia, roughly along Guangchang–Xunwu fault zone (Fig. 1b), with the occurrence of Mesozoic I-type granites mainly to the southeast and S-type granites mainly to the northwest (Chen and Jahn, 1998; Zheng et al., 2004; Xu et al., 2007; Chen et al., 2008b; Yu et al., 2011).

In the Nanling region, Sinian clastic sedimentary rocks, which have experienced variable degrees of low grade metamorphism, are common (Yao et al., 2011). These Sinian meta-sedimentary strata conformably overlie the metamorphosed Precambrian lithologies (Yu et al., 2010). Jurassic to Cretaceous granitoids are widespread and some of them host important metallic ore deposits (Hsieh et al., 2008). For example, numerous W-Sn-polymetallic ore deposits are spatially, temporally and genetically related to the widespread Late Jurassic granitoids (ca. 150–160 Ma) (Mao et al., 2007, 2008, 2013a,b; Feng et al., 2011, 2015; Guo et al., 2011; Hu and Zhou, 2012). The strongly peraluminous granitoids (A/CNK > 1.1) in the region are characterized by relatively high initial $^{87}Sr/^{86}Sr$ (> 0.71), low $\varepsilon_{Nd}(t)$ (< 10) and the presence of abundant inherited zircons, and mostly belong to the S-type according to the studies of most researchers (e.g., Lu, 1986; Hua et al., 2003; Mao et al., 2008; Wang, 2008; Feng et al., 2011, 2015). The in situ zircon Hf-O isotope analysis realizes that the S-type granitic magma in this region does not totally preclude mantle contribution (e.g., Jiao et al., 2015; Gao et al., 2016), because the mantle-derived magma underplating under lithospheric extension is thought to be the dominant heat source for the S-type granitic magmatism (e.g., Clemens, 2003; Huang et al., 2013; Wang et al., 2013).

2.2. Deposit geology

The Xihuashan W deposit is a vein-type hydrothermal deposit, occurring in the Chong-You-Yu ore cluster. In the ore cluster, Cambrian low-grade meta-sandstone and slate were intruded by a Late Jurassic granitoid batholith that consists of multiple plutons (ca. 155.6 ± 1.9–158.7 ± 0.7 Ma; Li et al., 2013; Yang et al., 2018) (Fig. 2), with compositions varying from medium-grained porphyritic biotite granite to medium-grained biotite granite, plus minor fine-grained two-mica granite (Guo et al., 2012; Yang et al., 2012). The W-mineralized veins are spatially associated with the medium-grained biotite granites (Fig. 2). Whole-rock chemical and isotopic data indicate that these rocks are strongly peraluminous, belong to the S-type (e.g., Wu et al., 1987; Shen et al., 1994; Zeng et al., 2001; Xiao et al., 2009; Lü et al., 2011) derived from a reduced (fO_2 < ΔFMQ + 0, (ΔFMQ −10 to −3)) magma mainly due to partial melting of the Proterozoic basement with minor mantle contribution (Yang et al., 2018).

The Xihuashan W ore deposit comprises more than 700 W-bearing veins (Hu et al., 2012b; Wei et al., 2012). They occur in two groups with different orientations, i.e., an EW-trending, steeply dipping (75–85°) group in north and an NEE-trending, steeply diping (80–85°) group in the south (Giuliani et al., 1988; Wei et al., 2012). Within each group, the veins are sub-parallel. An echelon structure is common in the veins of both groups. Individual veins are mostly 200–600 m in length and 0.2–0.6 m in thickness, with downward extension mostly from 60 to 200 m and rarely > 350 m (Wu et al., 1987; Giuliani et al., 1988; Wei et al., 2012). Ore minerals in the veins are mainly wolframite and molybdenite, with minor arsenopyrite, cassiterite, pyrite and chalcopyrite (Fig. 3). Gangue minerals are predominately quartz, with minor muscovite, feldspar, fluorite, beryl and calcite (Hu et al., 2012b; Wei et al., 2012). Based on variations in mineral assemblages, crosscutting relationships and ore textures, the following paragenetic sequence is deduced for the veins: early silicate-oxide stage, middle sulfide stage, and late carbonate stage (Tanelli, 1982; Lu, 1986; Wu et al., 1987; Giuliani et al., 1988; Chang et al., 2007). Features of each stage are summarized in Fig. 4. The silicate-oxide stage produced massive wolframite and minor arsenopyrite or pyrite. The sulfide stage produced pyrite, arsenopyrite and rare wolframite (Wu et al., 1987; Wei et al., 2012). The hydrothermal alteration in different mineralization stages is quite similar (Wu et al., 1987; Chang et al., 2007). Greisen-, potassic-, silicic- and sericite alteration, were well developed at the contacts with country rocks (Wu et al., 1987). K-feldspar alteration and greisenization are intensive and pervasive, and closely W mineralization-related (Chen and Zhang, 1990). Greisenization and potassic alteration comprise muscovite ± quartz + wolframite ± sulfide and K-feldspar ± quartz + muscovite + wolframite ± sulfide, respectively (Wu et al., 1987). The age of W-mineralization was determined to be 157.8 ± 0.9 Ma based on molybdenite Re-Os method and 152.8 ± 1.6 Ma based on muscovite Ar-Ar method (Hu et al., 2012b). These ages are indistinguishable with the zircon U-Pb age of 156.0 ± 4 Ma for the associated granite (Liu et al., 2002). Coexisting vapor-rich and liquid-rich fluid inclusions in quartz have similar homogenization temperatures, indicating that boiling may have taken place during quartz crystallization (Wei et al., 2012). However, the absence of vapor-rich fluid inclusions in coexisting pyrite and wolframite in the veins (Huang et al., 2012) indicates that boiling was not important during the deposition of pyrite and wolframite (Wei et al., 2012). The fluid inclusions entrapped in the minerals formed at the silicate-oxide stage have the homogenization temperatures from ~236 to 380 °C and salinities of 1.2–13.7 wt% NaCl equivalent; the fluid inclusions entrapped in the quartz have lower homogenization temperatures from 177 to 241 °C and lower salinities from 0.9 to 5.1 wt% NaCl equivalent (Wei et al., 2012).

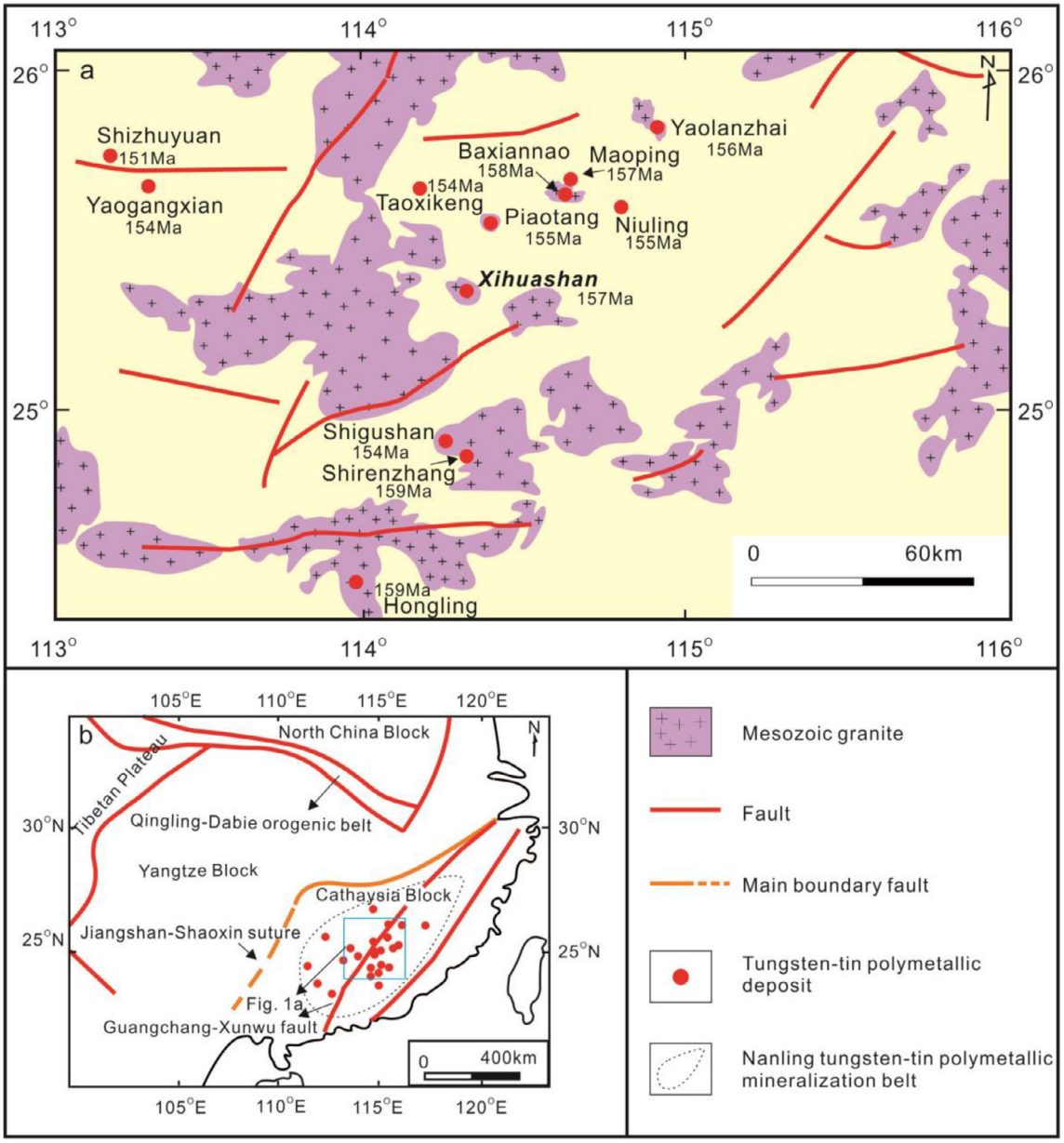

Fig. 1. Distribution of major W deposits in the central Nanling region, South China (modified from Hu et al., 2012b).

3. Sampling and methodology

Arsenopyrite and pyrite separates (Fig. 3) from wolframite-bearing samples from the Xihuashan W ore deposit were analyzed for the He and Ar isotopes. The samples were collected from underground mining channels at different elevations (270, 378, 431 and 538 m). The samples were crushed to 1–3 mm and the mineral separates were hand-picked under a binocular microscope. Eight samples of the silicate-oxide stage and seven samples of the sulfide stage are used in this study (Table 1).

The noble gas isotopes of volatiles released from the mineral separates were analyzed by gas mass spectrometry (GV 5400; with an all metal extraction system) at the Institute of Geochemistry, Chinese Academy of Sciences in Guiyang (IGCAS). The analytical procedures were similar to those described by Stuart et al. (1994, 1995) and Hu et al. (2012a). Approximately 0.5–1 g of arsenopyrite and pyrite separates with diameters from 0.5 to 1.5 mm were cleaned ultrasonically in acetone for 20 min followed by several runs of washing using distilled water and ethanol, then dried, and finally loaded into the online vacuum crushing device. The samples of pre-treated mineral separates were heated at ~150 °C in ultra-high vacuum for 24 h to remove adhered atmospheric contaminants before analysis. The inclusion-hosted noble gases in the sulfide crystals were extracted by sequential crushing in modified Nupro valves. A two-stage gas clean-up procedure was employed. In the first stage, a Ti sponge furnace at 800 °C for 20 min was used to remove the bulk of active gases (e.g., H_2O and CO_2). In the second stage the SAES Zr-Al getters, one at room temperature and the other at 450 °C for 10 min each, were used to further purify the samples. This was followed by the sequential trapping of Ar into an activated charcoal cold finger at liquid nitrogen temperature (−196 °C) and He into an activated charcoal finger at a higher temperature. Helium was released from the cryogenic finger, and its abundance and isotope compositions determined using a GV 5400 noble gas mass spectrometry. This was followed by the analyses for Ar. The abundance of noble gas was measured by peak-height comparison with accurately known amount of standard air. Helium and Ar abundance and isotopic ratios were calibrated against pipettes of 0.1 cm^3 STP air (5.2×10^{-7} cm^3 STP ^{4}He and 9.3×10^{-4} cm^3 STP ^{40}Ar). Procedural

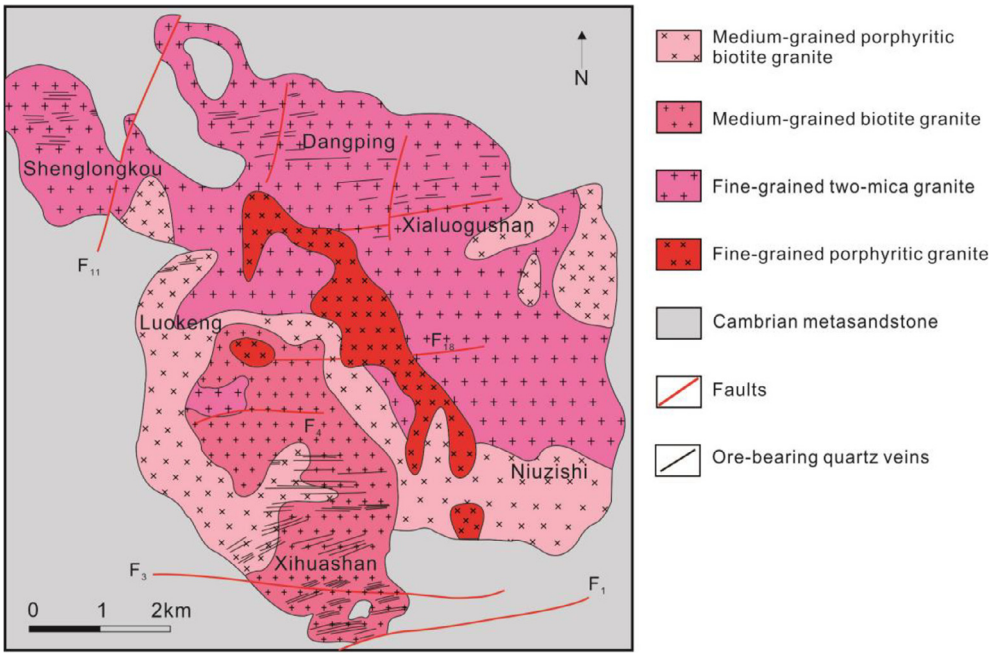

Fig. 2. Geological map of the Xihuashan W deposit (modified from Zhang et al., 2018).

blank contributions ($< 2 \times 10^{-10}$ cm^3 STP ^{4}He, (2–4) $\times 10^{-10}$ cm^3 STP ^{40}Ar, constituting < 1% of the analytical results) were insignificant.

4. Results

One disadvantage of the crushing analytical technique is that it is difficult to separate different generations of fluid inclusions in a sample of mineral separates. Consequentially, the analytical results represent an average composition of all fluid inclusions crushed (Burnard and Polya, 2004). Both the fluid inclusion density in the minerals, and the efficiency and processes of the *in vacuum* crushing would affect the estimation of He-Ar concentrations in sulfides, and therefore measured He-Ar concentrations are semi-quantitative (e.g., Burnard et al., 1999) and may have little geological significance (Kendrick and Burnard, 2013). In contrast, the He and Ar isotopes of the crushed fluid inclusions can be used to determine the mantle and atmospheric inputs to crustal fluids (Kendrick and Burnard, 2013). Table 1 lists the He and Ar isotope ratios for the crushed fluid inclusions in pyrite and arsenopyrite from the Xihuashan deposit. The ^{3}He/^{4}He ratios for these samples are 0.15–1.16 Ra, with a mean of 0.72 Ra. The ^{40}Ar/^{36}Ar ratios for these samples are ~306 to 1023, with an average of 440. The ^{40}Ar*/^{4}He

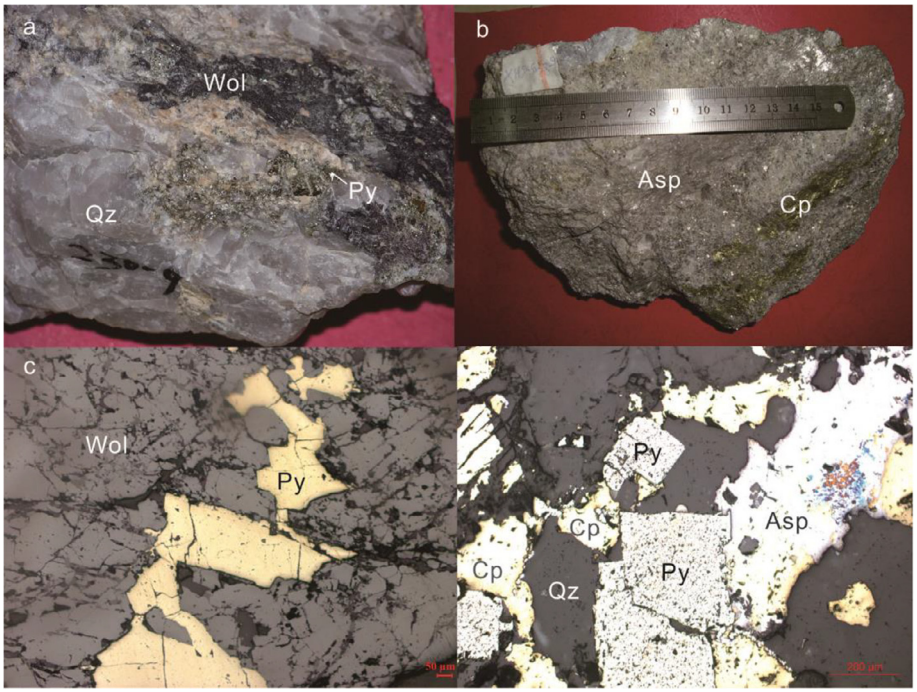

Fig. 3. Photographs (a-b) and photomicrographs (c-d) of ore minerals. Wol = wolframite, Qz = quartz, Py = pyrite, Cp = chalcopyrite, Asp = arsenopyrite, Photomicrograph d from Wei et al. (2012).

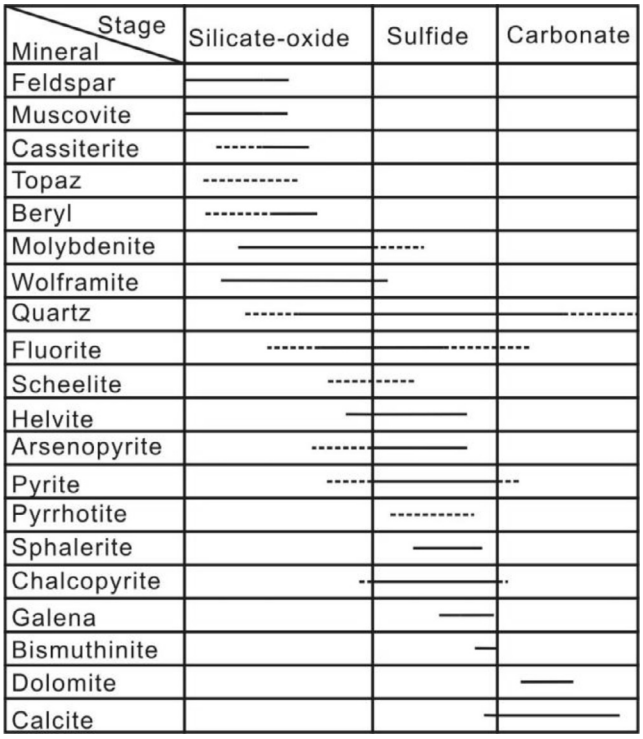

Fig. 4. Paragenetic sequence of minerals from the Xihuashan tungsten deposit (modified from Wei et al., 2012).

[$^{40}Ar^{*}$ is non-atmospheric Ar, calculated assuming that all ^{36}Ar is atmospheric in origin, i.e. $^{40}Ar^{*} = {}^{40}Ar - ({}^{36}Ar \times 295.5)$] and $^{3}He/^{36}Ar$ are from 0.008 to 0.481 and from 0.18×10^{-3} to 6.39×10^{-3}, respectively.

5. Discussion

5.1. The sources of He–Ar volatiles released from the crushed minerals

The He-Ar isotope compositions of primary fluid inclusions in pyrite and arsenopyrite are useful tracers for the sources of fluids. The measured $^{3}He/^{4}He$ and $^{40}Ar/^{36}Ar$ values of different crushing steps (i.e., crushing 1, crushing 2, etc.) are generally within error, and there is no distinct decrease in $^{3}He/^{4}He$ and $^{40}Ar/^{36}Ar$ with increasing degree of crushing. Our new He-Ar isotope compositions for the crushed fluid inclusions in the mineral separates from the Xihuashan W ore deposit mainly represent initial He and Ar compositions of the ore-forming fluids because (i) the majority of the fluid inclusions entrapped in the sulfides are primary rather than secondary (Huang et al., 2012), (ii) fluid inclusions in the sulfides have high degrees of He and Ar retention (Burnard et al., 1999; Zhang et al., 2011; Hu et al., 2012a), (iii) the samples were collected from underground, precluding significant cosmogenic ^{3}He (Burnard et al., 1999; Kendrick et al., 2011), (iv) contribution of ^{3}He from ^{6}Li decay is negligible because Li-rich minerals are absent in the samples (Wu et al., 1987), (v) *in-situ* generated radiogenic ^{4}He and ^{40}Ar after fluid entrapment as primary inclusions were also negligible (Burnard and Polya, 2004; Graupner et al., 2006; Kendrick et al., 2006, 2007) and the crush-released noble gases were largely derived from fluid inclusions instead of impurities of the host minerals that may contain large amounts of *in-situ* produced radiogenic noble gasses (Burnard et al., 1999; Kendrick et al., 2011), (vii) isotope fractionation during He-leakage can be ruled out because preferential escape of ^{3}He over ^{4}He would produce lower $^{3}He/^{4}He$ (Kendrick et al., 2005; Bouabdellah et al., 2015) instead of the observed elevated values (Table 1).

The measured $^{40}Ar/^{36}Ar$ ratios are commonly significantly lower than the actual $^{40}Ar/^{36}Ar$ of the crushed fluid inclusions, mainly due to contribution of atmospheric Ar during sample preparation or analysis (Burnard et al., 1999; Kendrick et al., 2005). Although careful analytical procedures can minimize atmospheric Ar absorbed on the surfaces of the samples and the crushing apparatus, air-derived contamination is difficult to be entirely eliminated. Therefore, the actual $^{40}Ar/^{36}Ar$ of the fluid inclusions in the minerals must be higher than the highest measured values (Kendrick et al., 2001; Hu et al., 2012a). However, the observed variation of $^{40}Ar/^{36}Ar$ from sample to sample may be in part related to variable $^{40}Ar/^{36}Ar$ in the fluids entrapped in different samples (Hu et al., 2012a).

5.2. Origin of He and Ar

Noble gas Isotopes can be used to quantitatively trace the sources of volatiles in ore-forming fluids (Stuart et al., 1994; Kendrick et al., 2001) and constrain the fluid-rock interaction (Bouabdellah et al., 2015). He and Ar isotopes have been widely used to determine the fluid sources (Turner et al., 1993; Hu et al., 1998b; Burnard et al., 1999; Kendrick and Burnard, 2013). Helium has an extremely low abundance in the atmosphere and a low solubility in aqueous fluids (Stuart et al., 1994), leaving only two possible sources for the He in hydrothermal fluids, i.e., mantle-derived He and radiogenic He produced in the crust (Turner et al., 1993; Hu et al., 2012a; Moura et al., 2014). The wide range of $^{3}He/^{4}He$ in the fluid inclusions in the sulfide separates from the Xihuashan W ore deposit indicates that various fluid sources were involved in the origin and evolution of the ore-forming fluids. The $^{3}He/^{36}Ar$ ratios of the volatiles released from the crushed fluid inclusions in the sulfides of the deposit ($0.18–6.39 \times 10^{-3}$) are five orders of magnitude higher than the value for air-saturated water ($\sim 5 \times 10^{-8}$), indicating negligible atmospheric contribution to the He in the Xihuashan ore-forming fluids. The $F^{4}He$ ($(^{4}He/^{36}Ar)_{sample}/(^{4}He/^{36}Ar)_{air}$, where $(^{4}He/^{36}Ar)_{air} = 0.1655$) for a sample containing 100% atmospheric He will have $F^{4}He = 1$ (Kendrick et al., 2001). The $F^{4}He$ for the Xihuashan samples are from 1928 to 47514 (Table 1), which are more than 4 orders of magnitude higher than the value for an atmospheric sample.

Mantle-derived fluids are high in ^{3}He and low in ^{36}Ar. $^{3}He/^{4}He > \sim 0.05$ Ra in hydrothermal fluids may indicate a contribution from a mantle-derived He flux (Oxburgh et al., 1986). Overall, the measured $^{3}He/^{4}He$ values for the volatiles released from crushed fluid inclusions in the sulfide separates from the Xihuashan deposit are much higher than the average crustal value (0.02 Ra; Ballentine and Burnard, 2002), but lower than that for the sub-continental lithospheric mantle (SCLM) (6.1 ± 0.8 Ra; Gautheron and Moreira, 2002). The mineral separates from each hand specimen yield a range of $^{3}He/^{4}He$ that can be explained by mixing between crustal radiogenic- and mantle-derived components. The observed high $^{3}He/^{36}Ar$ values for the Xihuashan ore-forming fluids (Table 1) and similarly high $^{3}He/^{36}Ar$ values for the W-mineralized granitoids (Fig. 5) indicates a common noble gas source for the ore-forming fluids and the associated granitoids as well as a significant mantle component in both systems. The $^{40}Ar/^{36}Ar$ ratios for the crushed fluid inclusions in the minerals separates from the Xihuashan deposit are from 306 to 1023, slightly higher than the atmospheric value (295.5) but lower than that for the MORB (10,000 to 40,000, Burnard et al., 1999), which indicates that the Xihuashan ore-forming fluids resulted from the mixing between mantle-derived and crustal fluids.

Pure air-saturated water is characterized by atmospheric He and Ar isotope compositions ($^{40}Ar/^{36}Ar = 295.5$ and $^{3}He/^{36}Ar = 5 \times 10^{-8}$) (Turner et al., 1993; Stuart et al., 1995; Burnard et al., 1999, 2013). Radiogenic ^{4}He and ^{40}Ar, produced by the decay of U, Th and K in the aquifer rocks, would diffuse into the groundwater and pore fluids (Elliot et al., 1993; Burnard et al., 1999). As a result, the crustal fluids were actually a mixture between air-saturated water and additional crustal radiogenic components, and were characterized by low $^{3}He/^{4}He$

Table 1
He and Ar isotopic compositions of inclusion-trapped fluid in pyrite and arsenopyrite from the Xihuashan tungsten deposit.

Sample	Min[a]	CN[b]	Weights[c]	^4He[d]	$^3He/^4He$	^{40}Ar	$^{40}Ar/^{36}Ar$	$^3He/^{36}Ar$	$^{40}Ar^*/^4He$	F^4He	^4He	^{40}Ar	$^3He/Q$
			(g)	(10^{-8} cm^3 STP)	(Ra)	(10^{-8} cm^3 STP)		(10^{-3})	(10^{-3})		(cm^3 STP/g)	(cm^3 STP/g)	(10^{-12} cm^3 STP J^{-1})
The silicate-oxide stage													
27-9	Apy	1		27.03 ± 0.96	0.88 ± 0.03	10.66 ± 0.35	355 ± 12	1.11 ± 0.08	65.86 ± 4.45	5434 ± 321			0.64
		2		19.13 ± 0.68	1.16 ± 0.04	5.42 ± 0.18	400 ± 20	2.29 ± 0.18	74.02 ± 5.74	8534 ± 598			1.33
		Total[e]	0.2771	46.15 ± 1.18	1.00 ± 0.04	16.08 ± 0.39	369 ± 17	1.48 ± 0.08	69.24 ± 3.57	6397 ± 290	1.67E−06	5.80E−07	0.86
538-3	Apy	1		23.60 ± 0.84	1.00 ± 0.04	19.28 ± 0.63	319 ± 4	0.55 ± 0.03	59.00 ± 3.53	2356 ± 118			0.32
		2		8.43 ± 0.30	1.12 ± 0.04	6.76 ± 0.22	334 ± 6	0.65 ± 0.04	91.89 ± 5.67	2512 ± 131			0.38
		Total[e]	0.1486	32.03 ± 0.89	1.03 ± 0.04	26.04 ± 0.67	322 ± 12	0.57 ± 0.03	67.65 ± 3.19	2395 ± 94	2.16E−06	1.75E−06	0.33
538-11	Apy	1		30.30 ± 1.08	0.97 ± 0.04	25.18 ± 0.83	337 ± 2	0.55 ± 0.03	101.63 ± 5.99	2448 ± 120			0.32
		2		10.00 ± 0.36	0.98 ± 0.04	ND[f]							
		Total[e]	0.2528	40.30 ± 1.14	0.97 ± 0.04						1.59E−06	9.96E−07	
538-9	Apy	1		36.33 ± 1.29	0.88 ± 0.03	34.42 ± 1.13	327 ± 3	0.43 ± 0.03	90.13 ± 5.34	2082 ± 103			0.25
		2		12.94 ± 0.46	0.80 ± 0.03	10.32 ± 0.34	308 ± 8	0.44 ± 0.03	33.08 ± 2.10	2335 ± 127			0.26
		Total[e]	0.2552	49.27 ± ± 1.37	0.86 ± 0.03	44.74 ± 1.18	322 ± 12	0.43 ± 0.02	75.15 ± 3.56	2143 ± 84	1.93E−06	1.75E−06	0.25
538-10	Apy	1		37.23 ± 1.33	0.76 ± 0.03	33.40 ± 1.10	315 ± 1	0.37 ± 0.02	54.50 ± 3.20	2119 ± 103			0.21
		2		12.33 ± 0.44	0.86 ± 0.03	10.19 ± 0.34	334 ± 8	0.49 ± 0.03	95.13 ± 5.98	2440 ± 131			0.28
		Total[e]	0.1506	49.55 ± 1.40	0.78 ± 0.03	43.59 ± 1.15	319 ± 12	0.40 ± 0.02	64.60 ± 3.05	2191 ± 86	3.29E−06	2.89E−06	0.23
538-18	Apy	1		24.86 ± 0.89	0.69 ± 0.03	25.71 ± 0.85	330 ± 2	0.31 ± 0.02	108.35 ± 6.38	1928 ± 94			0.18
		2		20.62 ± 0.73	0.97 ± 0.04	16.58 ± 0.55	339 ± 4	0.57 ± 0.04	104.05 ± 6.21	2550 ± 127			0.33
		Total[e]	0.2058	45.48 ± 1.15	0.82 ± 0.03	42.30 ± 1.01	334 ± 11	0.41 ± 0.02	106.40 ± 4.52	2168 ± 76	2.21E−06	2.06E−06	0.24
538-13	Apy	1		25.56 ± 0.93	1.12 ± 0.06	23.29 ± 0.78	331 ± 16	0.57 ± 0.03	98.19 ± 5.92	2195 ± 110			0.33
		2		21.66 ± 0.78	1.12 ± 0.06	13.93 ± 0.47	362 ± 18	0.88 ± 0.05	117.66 ± 7.26	3398 ± 176			0.51
		Total[e]	0.205	47.22 ± 1.21	1.12 ± 0.04	37.22 ± 0.91	342 ± 12	0.68 ± 0.03	107.12 ± 4.71	2621 ± 96	2.30E−06	1.82E−06	0.39
538-9	Py	1		43.41 ± 1.55	0.52 ± 0.02	15.43 ± 0.51	362 ± 5	0.75 ± 0.05	65.50 ± 3.93	6160 ± 309			0.43
		2		117.96 ± 4.20	0.57 ± 0.02	34.87 ± 1.15	407 ± 4	1.09 ± 0.07	80.71 ± 4.78	8309 ± 410			0.63
		Total[e]	0.1685	161.38 ± 4.48	0.55 ± 0.02	50.30 ± 1.25	392 ± 14	0.98 ± 0.05	76.62 ± 3.47	7596 ± 287	9.58E−06	2.98E−06	0.57
The sulfide stage													
431-32	Apy	1		110.38 ± 3.93	0.15 ± 0.01	38.12 ± 1.25	306 ± 1	0.18 ± 0.01	11.34 ± 0.66	5345 ± 259			0.13
		2		174.44 ± 6.21	0.25 ± 0.01	19.67 ± 0.65	344 ± 4	1.08 ± 0.07	15.96 ± 0.96	18443 ± 926			0.75
		Total[e]	0.1393	284.82 ± 7.35	0.21 ± 0.01	57.79 ± 1.41	318 ± 11	0.47 ± 0.02	14.17 ± 0.62	9460 ± 341	2.04E−05	4.15E−06	0.33
270-5	Apy	1		49.49 ± 1.79	0.43 ± 0.02	43.50 ± 1.45	660 ± 34	0.45 ± 0.03	485.15 ± 30.83	4535 ± 245			0.31
		2		130.76 ± 4.75	0.42 ± 0.02	17.01 ± 0.57	1023 ± 52	4.63 ± 0.25	92.54 ± 5.79	47514 ± 2504			3.22
		Total[e]	0.1815	180.25 ± 5.07	0.42 ± 0.02	60.51 ± 1.56	733 ± 31	1.29 ± 0.06	200.35 ± 10.11	13189 ± 572	9.93E−06	3.33E−06	0.90
270-13	Apy	1		36.20 ± 1.32	0.54 ± 0.03	13.17 ± 0.45	464 ± 27	0.96 ± 0.06	131.93 ± 9.02	7704 ± 456			0.67
		2		42.59 ± 1.54	0.61 ± 0.03	13.28 ± 0.44	547 ± 30	1.49 ± 0.09	143.42 ± 9.37	10599 ± 595			1.04
		Total[e]	0.1509	78.79 ± 2.03	0.58 ± 0.02	26.45 ± 0.63	502 ± 20	1.20 ± 0.05	138.14 ± 6.56	9038 ± 371	5.22E−06	1.75E−06	0.83
270-10	Py	1		116.71 ± 4.15	0.52 ± 0.02	22.29 ± 0.73	576 ± 11	2.19 ± 0.14	92.92 ± 5.71	18213 ± 944			1.52
		2		153.35 ± 5.46	0.52 ± 0.02	25.71 ± 0.85	657 ± 10	2.82 ± 0.18	92.21 ± 5.57	23671 ± 1198			1.96
		3		71.07 ± 2.53	0.56 ± 0.02	11.08 ± 0.36	683 ± 33	3.46 ± 0.27	88.53 ± 6.68	26477 ± 1799			2.41
		Total[e]	0.3898	341.13 ± 7.31	0.53 ± 0.02	59.08 ± 1.18	628 ± 19	2.67 ± 0.10	91.68 ± 3.46	21908 ± 701	8.75E−06	1.52E−06	1.86
270-23	Py	1		86.19 ± 3.10	0.84 ± 0.03	14.13 ± 0.47	692 ± 36	4.91 ± 0.40	95.14 ± 7.47	25189 ± 1797			3.41
		2		148.40 ± 5.31	0.77 ± 0.03	26.25 ± 0.86	611 ± 9	3.74 ± 0.23	91.13 ± 5.52	20936 ± 1065			2.60
		3		28.41 ± 1.01	1.06 ± 0.04	4.05 ± 0.13	613 ± 21	6.39 ± 0.44	73.8 ± 4.99	26030 ± 1537			4.44
		Total[e]	0.3435	263.40 ± 6.23	0.82 ± 0.03	44.60 ± 0.99	635 ± 23	4.33 ± 0.19	90.57 ± 3.94	22666 ± 848	7.67E−06	1.30E−06	3.01
378-9	Py	1		45.80 ± 1.63	0.50 ± 0.02	11.40 ± 0.38	451 ± 6	1.26 ± 0.08	85.83 ± 5.15	10945 ± 549			0.88
		2		89.63 ± 3.20	0.51 ± 0.02	22.48 ± 0.74	469 ± 3	1.33 ± 0.08	92.73 ± 5.46	11292 ± 552			0.92
		3		83.92 ± 2.99	0.37 ± 0.01	11.41 ± 0.38	572 ± 17	2.17 ± 0.15	65.74 ± 4.30	25432 ± 1436			1.51
		Total[e]	0.3623	219.35 ± 4.67	0.45 ± 0.01	45.30 ± 0.91	486 ± 14	1.49 ± 0.06	80.97 ± 2.96	14223 ± 433	6.05E−06	1.25E−06	1.04
431-4	Py	1		141.22 ± 5.03	0.72 ± 0.03	25.61 ± 0.84	664 ± 5	3.69 ± 0.22	100.70 ± 5.94	22137 ± 1085			2.57
		2		43.96 ± 1.57	0.73 ± 0.03	8.60 ± 0.28	569 ± 21	2.96 ± 0.21	94.10 ± 6.52	17578 ± 1072			2.06

(*continued on next page*)

Table 1 (*continued*)

Sample	Min[a]	CN[b]	Weights[c]	^{4}He[d]	^{3}He/^{4}He	^{40}Ar	^{40}Ar/^{36}Ar	^{3}He/^{36}Ar	^{40}Ar*/^{4}He	F^{4}He	^{4}He	^{40}Ar	^{3}He/Q
			(g)	(10^{-8} cm^3 STP)	(Ra)	(10^{-8} cm^3 STP)		(10^{-3})	(10^{-3})		(cm^3 STP/g)	(cm^3 STP/g)	(10^{-12} cm^3 STP J^{-1})
	Total[e]		0.1455	185.18 ± 5.27	0.72 ± 0.03	34.21 ± 0.89	638 ± 24	3.48 ± 0.17	99.14 ± 4.72	20853 ± 831	1.27E−05	2.35E−06	2.42

^{3}He/Q = ^{3}He/^{36}Ar × [^{36}Ar]$_{MASW}$/(C_pθ), where [^{36}Ar]$_{MASW}$ is the concentration of ^{36}Ar in modified air saturated water (7.65×10^{-7} cm^3 STP g^{-1}), C_p is the specific heat of MASW (4.4 J K^{-1} g^{-1}), and θ which is represented by fluid inclusion homogenization temperatures in coexisting gangue minerals of the same mineralizing stage (e.g., Wei et al., 2012) is the temperature increase of the cold fluid (°C) (Burnard and Polya, 2004).

[a] Mineral.
[b] Crushing number.
[c] Sample weights are the < 100 μm fraction after crushing.
[d] Errors quoted are at the 1σ confidence level.
[e] Totals are the sums of all crushes.
[f] Not determined; Apy-arsenopyrite; Py-pyrite.

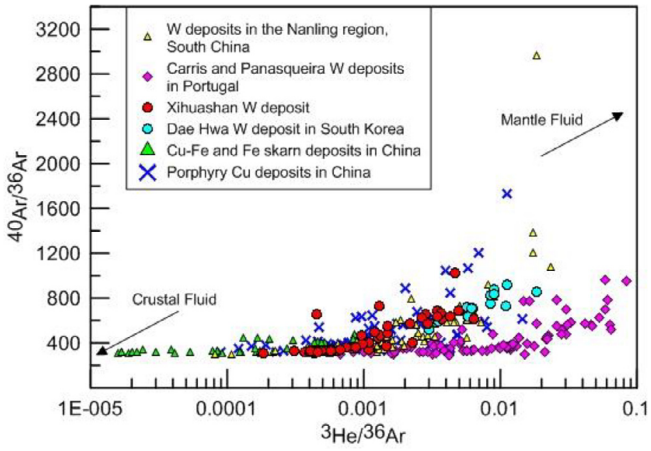

Fig. 5. ^{40}Ar/^{36}Ar vs. ^{3}He/^{36}Ar plot of the inclusion-trapped fluids from the Xihuashan W deposit. For comparison, shown are He–Ar isotopic compositional fields of porphyry Cu deposits in SW China (Hu et al., 1998a, 2004; Xu et al., 2014), the W deposits in the Nanling region (Wang et al., 2010; Wu et al., 2011; Hu et al., 2012b; Zhai et al., 2012), Portugal (Panasqueira deposit from Burnard and Polya, 2004; Carris deposit from Moura et al., 2014), and South Korea (Dae Hwa deposit from Stuart et al., 1995) are shown for comparison.

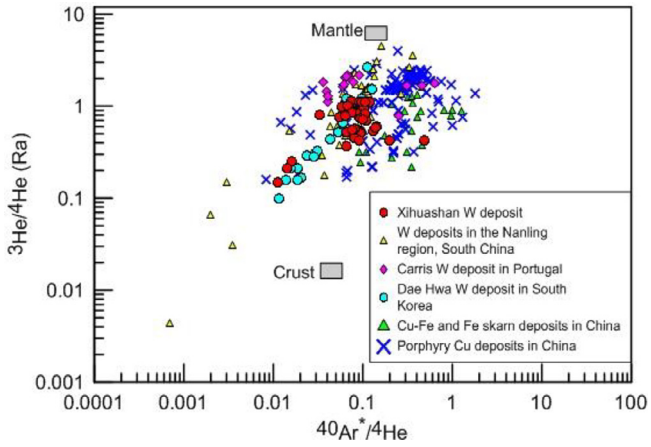

Fig. 6. ^{3}He/^{4}He vs. ^{40}Ar*/^{4}He plot of FIs from the Xihuashan W deposit. The fields for the average crust (^{3}He/^{4}He = 0.02 Ra, ^{40}Ar*/^{4}He = 0.2) and mantle (^{3}He/^{4}He = 6.1 ± 8 Ra; ^{40}Ar*/^{4}He = 0.69 ± 0.06) are from Gautheron and Moreira (2002), Ballentine et al. (2002). Data source and symbols are the same as in Fig. 5.

(0.001–0.05 Ra) and ^{3}He/^{36}Ar (< $\times 10^{-7}$), and near-atmospheric ^{40}Ar/^{36}Ar (295.5), and could be described as modified air-saturated water (MASW) (e.g., Stuart et al., 1995; Burnard et al., 1999; Hu et al., 2004, 2009, 2012a; Xie et al., 2016). As shown in Fig. 6, the ^{40}Ar*/^{4}He values of the crustal fluid end member are below the crustal production ratio of ~0.2 (Ballentine and Burnard, 2002), reflecting the preferential acquirement of ^{4}He relative to ^{40}Ar from crustal rocks and low temperature characteristics of MASW (Hu et al., 2004, 2012a; Kendrick et al., 2005).

Due to the lack of He isotope data for Mesozoic mafic rocks in South China, the highest ^{3}He/^{4}He (6.64 Ra) of the mantle-derived xenoliths in the Cenozoic Lianshan basalts from Yangtze craton (Correale et al., 2016), within the typical SCLM range (6.1 ± 0.8 Ra; Gautheron and Moreira, 2002), was taken to represent the SCLM value of the late Mesozoic W deposits in South China. A simple two-component mixing model between the mantle (6.64 Ra) and crustal He (0.02 Ra) indicates that the contributions of mantle-derived He in the Xihuashan ore-forming fluids were likely to be in the range of ~2 to 17%.

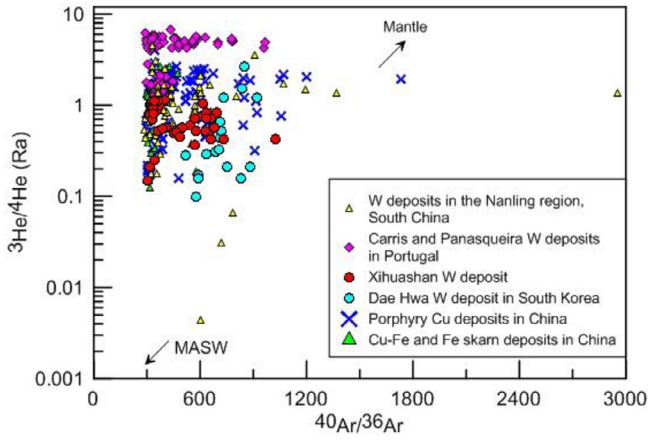

Fig. 7. $^{40}Ar/^{36}Ar$ vs. $^3He/^4He$ (Ra) plot of the inclusion-trapped fluids from the Xihuashan W deposit. Data source and symbols are the same as in Fig. 5.

5.3. Granitic magma and mantle-derived noble gases

In the Xihuashan hydrothermal W deposit, $^3He/^4He$ and $^{40}Ar/^{36}Ar$ are from 0.15 to 1.16 Ra and from 306 to 1023, respectively, which indicates mixing between MASW and a fluid with a mantle component. These values are consistent with different proportion of mantle-derived components within the formation of the Cu–Fe and Fe skarn deposits (e.g., Xie et al., 2016) and the porphyry Cu deposits in Southwest China (e.g., Hu et al., 1998a,b, 2004; Xu et al., 2014) (Figs. 5–7). He–Ar isotopic compositions are also similar to those for several granite-related W deposits in South China, Korea and Portugal (Stuart et al., 1995; Burnard and Polya, 2004; Wu et al., 2011; Hu et al., 2012a; Moura et al., 2014) (Figs. 5–7). One of the hydrothermal deposits with the highest mantle contribution to the ore-forming fluids reported to date is the Panasqueira W deposit in Portugal which is characterized by Ra > 5, corresponding to 75% mantle component in the fluids. Since the magma of the granitoids associated with this deposit was predominantly crustally derived, such extremely high proportion of mantle-derived He in the fluids required an independent mantle source (Burnard and Polya, 2004). However, no independent mantle source is required for the Xihuashan deposit because the proportion of mantle-drived He in this deposit is much lower (only ~2 to 17%) and similar to that in the associated granite pluton. In addition, the C-S isotopes of the deposit and the associated granitoids are also consistent each other. The $\delta^{34}S$ and $\delta^{13}C$ values of hydrothermal sulfides and calcites are from −1.6 to +0.1‰ and from −4.5 to −7.5‰, respectively (Wu et al., 1987; Wei et al., 2012), indicating that the sulfur and CO_2 in the fluids were mainly derived from the associated granitoids during magma evolution. The H and O isotope data for the deposit are consistent with the interpretation that the ore-forming fluids formed by mixing between magmatic fluids and meteoric water (Mu et al., 1981; Zhang et al., 1981; Liu et al., 2002; Wei et al., 2012). Therefore, we propose that the mantle end-member in the ore-forming fluids of the Xihuanshan W deposit was inherited from the magmatic fluids of the associated granitoids.

In most magmatic hydrothermal ore deposits, He and Ar isotopes of inclusion-trapped fluids are significantly lower than their potential sources in the SCLM (e.g., Kendrick and Burnard, 2013; Xie et al., 2016). This may have resulted from two processes, (1) source mixing of radiogenic- and mantle-derived noble gases in the magma, and (2) dilution of hydrothermal fluids by MASW (e.g., Hu et al., 2009, 2012a). Before the exsolution of hydrothermal fluids, radiogenic He might be added to the magma *via* crustal assimilation or magma evolution processes in a long-lived magma chamber (Simmons et al., 1987; Graupner et al., 2006). The underplating of mantle-derived magma might cause partial melting of the overlying crust (Huppert and Sparks, 1988). The mixed magma produced by this process could ultimately produce a magmatic fluid with both crustal and mantle He isotopic signatures (Stuart et al., 1995). Alternatively, magmatic fluids with strong crustal and minor mantle-derived He isotopic signatures might have resulted from a heterogenous protolith that was dominated by an old crust but also contained minor amount of jevinile igneous rocks with a mantle origin (Hu et al., 2012a). As described above, the observed elevated $^3He/^4He$ (~0.15 to 1.16 Ra; Table 1) for the Xihuashan W ore deposit is consistent with the involvement of ~2 to 17% mantle-derived He. It is difficult to distinguish the above-mentioned possibilities for the derivation of the mantle noble gasses in the ore-forming fluids of the deposit, owing to the fact that there is no significant He-Ar isotopic fractionation between magma and fluids in a magmatic hydrothermal system (Turner et al., 1993; Graham, 2002; Hu et al., 2004; Kendrick et al., 2007).

The Xihuashan granite pluton is a typical W-bearing granite pluton in South China. Since the 1980s, many studies have investigated the mineralogy, petrology, geochemistry, and isotopes of this pluton (e.g. McKee et al., 1987; Wu et al., 1987; Shen et al., 1994; Xiao et al., 2009; Zhou et al., 2010; Wang et al., 2011). Whether or not mantle-derived materials were involved in the formation of Xihuashan granite pluton is still debated. Recently, zircon Hf-O ($\delta^{18}O$: mainly 6.93 to 10.40‰; εHf (t): mainly –5 to –15‰) isotope data and Sr-Nd isotope data clearly indicate the minor involvement of mantle components in the magma of the Xihuashan granite pluton (Guo et al., 2012), because solely crust-derived granitoids produced by partial melting of metasedimentary rocks without mantle input mostly have $\delta^{18}O$ values higher than 10‰ (Jo et al., 2018). Based on these results, some researchers proposed that this pluton was the product of crustal melt derived from the Paleo-proterozoic-Mesoproterozoic meta-sedimentary rocks, mixed with the underplating mantle-derived magma (Yang et al., 2012). It is suggested that such magmatic event was related to the tectonic evolution of South China and that from 160 to 150 Ma South China underwent lithospheric extension-thinning coupled with mantle upwelling (Mao et al., 2007, 2008, 2013a,b; Hu et al., 2012b). According to this model, partial melting of the crust was triggered by underplating of the mantle-derived magma generated by mantle upwelling. Evidence for the existance of the mantle-derived magma includes widespread coeval mafic dykes and intermediate igneous complexes in the Nanling region (Zhu et al 2009). The influx of mafic magma could be highly efficient to provide the heat input which induces partial melting of the crust (Annen and Sparks, 2002; Clemens, 2003). The estimated $^3He/Q$ ratio for Xihuashan fluids ranging from 0.13 to 4.44 × 10^{-12} cm^3 STP J^{-1} (Table 1) are 2 to 40 times higher than those recorded by hydrothermal fluids from mid-oceanic ridges (0.1–0.2 × 10^{-12} cm^3 STP J^{-1}) (Baker and Lupton, 1990; Lupton et al., 1989) and slightly lower than those of the granite-related Panasqueria W deposit (up to 10 × 10^{-12} cm^3 STP J^{-1}, Burnard and Polya, 2004). The $^3He/^{40}Ar^*$ ratio of the samples range from 0.2 to 3.4 × 10^{-5}, close to that of mantle value (~10^{-4}, Kennedy et al., 1991) and far higher than that of the crust value (~10^{-8}, Kennedy et al., 1991). The high $^3He/Q$ and near mantle $^3He/^{40}Ar^*$ ratios of the mineralizing fluids indicate that mantle could provide heat and volatiles (e.g., Wu et al., 2011).

As described above, the Xihuashan W ore deposit was not only spatially but also temporally related to the granite pluton. We propose that small amount of mantle-derived He in the ore-forming fluids was inherited from the exsolved magmatic fluids from the granite pluton. Therefore, it is inferred that the host granite pluton was not the product of pure crustal melts proposed previously. Small amount of mantle-derived heat and volatiles were involved in the formation of this granite pluton.

6. Conclusions

Crushed fluid inclusions entrapped in sulfide minerals separated from the Xihuashan W ore deposit are characterized by $^3He/^4He$ from

0.15 to 1.16 Ra and $^{40}Ar/^{36}Ar$ from 306 to 1023. The results show that the released volatiles are mixtures of magmatic fluids with the so-called modified air-saturated water (MASW) and that the magmatic fluids contain small amount of mantle-derived He up to 17%. We propose that the mantle-derived He in the ore-forming fluids of the deposit was derived from the magma of the host granite pluton and that the parental magma of this pluton was generated by crust-mantle interaction in an extension tectonic environment.

Acknowledgements

The authors are grateful to the Xihuashan Mining Co. Ltd. for supporting the field work and to Dr. Guiqing Xie for his help in analysis. We are indebted to Dr. Chusi Li of Indiana University who read and revised the early versions of this manuscript. This research was jointly funded by the Strategic Priority Research Program (B) of Chinese Academy of Sciences (XDB18000000), the CAS/SAFEA International Partnership Program (KZZD-EW-TZ-20), the National Basic Research Program of China (2014CB440900) and the National Natural Science Foundation of China (41230316, 41203034, 41303030). The constructive comments from Prof. Franco Pirajno and two anonymous reviewers are deeply appreciated.

References

Annen, C., Sparks, R.S.J., 2002. Effects of repetitive emplacement of basaltic intrusions on thermal evolution and melt generation in the crust. Earth Planet. Sci. Lett. 203, 937–955.
Baker, E.T., Lupton, J.E., 1990. Changes in submarine hydrothermal 3He/heat ratios as an indicator of magmatic/tectonic activity. Nature 346, 556–558.
Ballentine, C.J., Burgess, R., Marty, B., 2002. Tracing fluid origin, transport and interaction in the crust. Rev. Mineral Geochem. 47, 539–614.
Ballentine, C.J., Burnard, P.G., 2002. Production, release and transport of noble gases in the continental crust. Rev. Mineral Geochem. 47, 481–538.
Bouabdellah, M., Niedermann, S., Velasco, F., 2015. The Touissit-Bou Beker Mississippi Valley-Type district of Northeastern Morocco: relationships to the Messinian salinity crisis, late Neogene-Quaternary alkaline magmatism, and buoyancy-driven fluid convection. Econ. Geol. 110, 1455–1484.
Burnard, P.G., Zimmermann, L., Sano, Y., 2013. The noble gases as geochemical tracers: history and background. In: The Noble Gases as Geochemical Tracer. Springer, Berlin Heidelberg, pp. 1–15.
Burnard, P.G., Hu, R.Z., Turner, G., Bi, X.W., 1999. Mantle, crustal and atmospheric noble gases in Ailaoshan gold deposits, Yunnan Province, China. Geochim. Cosmochim. Acta 63, 1595–1604.
Burnard, P.G., Polya, D.A., 2004. Importance of mantle derived fluids during granite associated hydrothermal circulation: He and Ar isotopes of ore minerals from Panasqueira. Geochim. Cosmochim. Acta 68, 1607–1615.
Chang, H.L., Wang, X.W., Wang, X.D., Liu, J.Q., Huang, H.L., 2007. The composition of melt inclusions in beryl from wolframite-quartz veins in Xihuashan, Jiangxi Province. Acta Petrol Mineral 26, 259–268 (in Chinese with English abstract).
Chen, C.H., Lee, C.Y., Shinjo, R., 2008a. Was there Jurassic paleo-Pacific subduction in South China?: constraints from $^{40}Ar/^{39}Ar$ dating, elemental and Sr-Nd-Pb isotopic geochemistry of the Mesozoic basalts. Lithos 106, 83–92.
Chen, J., Lu, J.J., Chen, W.F., Wang, R.C., Ma, D.S., Zhu, J.C., Zhang, W.L., Ji, J.F., 2008b. W-Sn-Nb-Ta-bearing granites in the Nanling Range and their relationship to metallogengesis. Geol. J. Chin. Univ. 14, 459–473 (in Chinese with English abstract).
Chen, J.F., Jahn, B.M., 1998. Crustal evolution of southeastern China: Nd and Sr isotopic evidence. Tectonophysics 284, 101–133.
Chen, Z.S., Zhang, L.G., 1990. Hydrogen and oxygen isotope study on altered rocks and it's geological significance: with the example of Xihuashan tungsten ore deposit. Contrib. Geol. Mineral Resour. Res. 5, 69–79 (in Chinese with English abstract).
Clemens, J.D., 2003. S-type granitic magmas—petrogenetic issues, models and evidence. Earth-Sci. Rev. 61, 1–18.
Correale, A., Rizzo, A.L., Barry, P.H., Lu, J., Zheng, J., 2016. Refertilization of lithospheric mantle beneath the Yangtze craton in south-east China: evidence from noble gases geochemistry. Gondwana Res. 38, 289–303.
Elliot, T., Ballentine, C.J., O'Nions, R.K., Ricchiuto, T., 1993. Carbon, helium, neon and argon isotopes in a Po basin (northern Italy) natural gas field. Chem. Geol. 106, 429–440.
Feng, C.Y., Zeng, Z.L., Zhang, D.Q., Qu, W.J., Du, A.D., Li, D.X., She, H.Q., 2011. SHRIMP zircon U-Pb and molybdenite Re–Os isotopic dating of the tungsten deposits in the Tianmenshan-Hongtaoling W–Sn orefield, southern Jiangxi Province, China, and geological implications. Ore Geol. Rev. 43, 8–25.
Feng, C.Y., Zhao, Z., Qu, W.J., Zeng, Z.L., 2015. Temporal consistency between granite evolution and tungsten mineralization in Huamei'ao, southern Jiangxi Province, China: evidence from precise zircon U-Pb, molybdenite Re–Os, and muscovite ^{40}Ar–^{39}Ar isotope geochronology. Ore Geol. Rev. 65, 1005–1020.
Gao, P., Zheng, Y.F., Zhao, Z.F., 2016. Distinction between S-type and peraluminous I-type granites: zircon versus whole-rock geochemistry. Lithos 258–259, 77–91.
Gautheron, C., Moreira, M., 2002. Helium signature of the subcontinental lithospheric mantle. Earth Planet. Sci. Lett. 199, 39–47.
Gilder, S.A., Gill, J., Coe, R.S., Zhao, X.X., Liu, Z.W., Wang, G.X., Yuan, K.R., Liu, W.L., Kuang, G.D., Wu, H.R., 1996. Isotopic and paleomagnetic constraints on the Mesozoic tectonic evolution of south China. J. Geophys. Res. 101, 16137–16154.
Giuliani, G., Li, Y.D., Sheng, T.F., 1988. Fluid inclusion study of Xihuashan tungsten deposit in the southern Jiangxi Province, China. Miner. Depos. 23, 24–33.
Graham, D.W., 2002. Noble gas isotope geochemistry of mid-ocean ridge and ocean island basalts: characterization of mantle source reservoirs. Rev. Mineral. Geochem. 47, 247–317.
Graupner, T., Niedermann, S., Kempe, U., Klemd, R., Bechtel, A., 2006. Origin of ore fluids in the Muruntau gold system: constraints from noble gas, carbon isotope and halogen data. Geochim. Cosmochim. Acta 70, 5356–5370.
Guo, C.L., Mao, J.W., Bierlein, F., Chen, Z.H., Chen, Y.C., Li, C.B., Zeng, Z.L., 2011. SHRIMP U-Pb (zircon), Ar–Ar (muscovite) and Re–Os (molybdenite) isotopic dating of the Taoxikeng tungsten deposit, South China Block. Ore Geol. Rev. 43, 26–39.
Guo, C.L., Chen, Y.C., Zeng, Z.L., Lou, F.S., 2012. Petrogenesis of the Xihuashan granites in southeastern China: constraints from geochemistry and in-situ analyses of zircon U-Pb-Hf-O isotopes. Lithos 148, 209–227.
Hsieh, P.S., Chen, C.H., Yang, H.J., Lee, C.Y., 2008. Petrogenesis of the Nanling Mountains granites from South China: constraints from systematic apatite geochemistry and whole-rock geochemical and Sr-Nd isotope compositions. J. Asian Earth Sci. 33, 428–451.
Hu, R.Z., Bi, X.W., Jiang, G.H., Chen, H.W., Peng, J.T., Qi, Y.Q., Wu, L.Y., Wei, W.F., 2012a. Mantle-derived noble gases in ore-forming fluids of the granite-related Yaogangxian tungsten deposit, Southeastern China. Miner. Depos. 47, 623–632.
Hu, R.Z., Bi, X.W., Turner, G., Burnard, P.G., 1999. He and Ar isotopic geochemistry of gold ore-forming fluids in the Ailaoshan gold mineralization belt. Sci. China Earth Sci. 29, 321–330 (in Chinese with English abstract).
Hu, R.Z., Burnard, P.G., Bi, X.W., Zhou, M.F., Peng, J.T., Su, W.C., Wu, K.X., 2004. Helium and argon isotope geochemistry of alkaline intrusion-associated gold and copper deposits along the Red River-Jinshajiang fault belt, SW China. Chem. Geol. 203, 305–317.
Hu, R.Z., Burnard, P.G., Bi, X.W., Zhou, M.F., Peng, J.T., Su, W.C., Zhao, J.H., 2009. Mantle-derived gaseous components in ore-forming fluids of the Xiangshan uranium deposit, Jiangxi province, China: evidence from He, Ar and C isotopes. Chem. Geol. 266, 86–95.
Hu, R.Z., Burnard, P.G., Turner, G., Bi, X.W., 1998a. Helium and Argon isotope systematics in fluid inclusions of Machangqing copper deposit in west Yunnan province, China. Chem. Geol. 146, 55–63.
Hu, R.Z., Turner, G., Burnard, P.G., Zhong, H., Ye, Z.J., Bi, X.W., 1998b. Helium and argon isotopic geochemistry of Jinding superlarge Pb-Zn deposit. Sci. China Ser. D-Earth Sci. 41, 442–448.
Hu, R.Z., Wei, W.F., Bi, X.W., Peng, J.T., Qi, Y.Q., Wu, L.Y., Chen, Y.W., 2012b. Molybdenite Re–Os and muscovite $^{40}Ar/^{39}Ar$ dating of the Xihuashan tungsten deposit, central Nanling district, South China. Lithos 150, 111–118.
Hu, R.Z., Zhou, M.F., 2012. Multiple Mesozoic mineralization events in South China—an introduction to the thematic issue. Miner. Depos. 47, 579–588.
Hua, R.M., Chen, P.R., Zhang, W.L., Liu, X.D., Lu, J.J., Lin, J.F., Yao, J.M., Qi, H.W., Zhang, Z.S., Gu, S.Y., 2003. Metallogenic systems related to Mesozoic and Cenozoic granitoids in South China. Sci. China Ser. D- Earth Sci. 46, 816–829.
Huang, H.L., Chang, H.L., Li, F., Zhang, C.H., Tan, J., Zhou, Y., 2012. A comparative study of fluid inclusions from coexisting transparent minerals and opaque minerals in Xihuashan tungsten deposit. Min. Depos. 31, 1171–1183 (in Chinese with English abstract).
Huang, H.Q., Li, X.H., Li, Z.X., Li, W.X., 2013. Intraplate crustal remelting as the genesis of Jurassic high-K granites in the coastal region of the Guangdong Province, SE China. J Asian Earth Sci. 74, 280–302.
Huppert, H.E., Sparks, R.S.J., 1988. The generation of granitic magmas by intrusion of basalt into continental crust. J. Petrol. 29, 599–624.
Jiao, S.J., Li, X.H., Huang, H.Q., Deng, X.G., 2015. Metasedimentary melting in the formation of charnockite: petrological and zircon U-Pb-Hf-O isotope evidence from the Darongshan S-type granitic complex in southern China. Lithos 239, 217–233.
Jo, H.J., Cheong, A.C.-S., Yi, K., Li, X.H., 2018. Juxtaposition of allochthonous terranes in the central Korean Peninsula: evidence from zircon U-Pb ages and O-Hf isotopes in Jurassic granitoids. Chem. Geol. 484, 136–147.
Kendrick, M.A., Burnard, P., 2013. Noble gases and halogens in fluid inclusions: a journey through the earth's crust. In: Burnard, P. (Ed.), The Noble Gases as Geochemical Tracers. Springer, Berlin, pp. 319–369.
Kendrick, M.A., Burgess, R., Harrison, D., Bjorlykke, A., 2005. Noble gas and halogen evidence for the origin of Scandinavian sandstone-hosted Pb-Zn deposits. Geochim. Cosmochim. Acta 69, 109–129.
Kendrick, M.A., Burgess, R., Pattrick, R.A.D., Turner, G., 2001. Fluid inclusion noble gas and halogen evidence on the origin of Cu-porphyry mineralising fluids. Geochim. Cosmochim. Acta 65, 2651–2668.
Kendrick, M.A., Duncan, R., Phillips, D., 2006. Noble gas and halogen constraints on mineralizing fluids of metamorphic versus surficial origin: Mt Isa, Australia. Chem. Geol. 235, 325–351.
Kendrick, M.A., Honda, M., Oliver, N.H.S., Phillips, D., 2011. The noble gas systematics of late-orogenic H_2O–CO_2 fluids, Mt Isa, Australia. Geochim. Cosmochim. Acta 75, 1428–1450.
Kendrick, M.A., Mark, G., Phillips, D., 2007. Mid-crustal fluid mixing in a Proterozoic Fe oxide-Cu-Au deposit, Ernest Henry, Australia: evidence from Ar, Kr, Xe, Cl, Br, and I. Earth Planet. Sci. Lett. 256, 328–343.
Kennedy, B.M., Hiyagon, H., Reynolds, J.H., 1991. Noble gases from Honduras

geothermal sites. J. Vocanol. Geotherm. Res. 45, 29–39.
Landis, G.P., Hofstra, A.H., 2012. Ore genesis constraints on the Idaho Cobalt Belt from fluid Iinclusion gas, noble gas isotope, and ion ratio analyses. Econ. Geol. 107, 1189–1205.
Li, Q.L., Li, X.H., Lan, Z.W., Guo, C.L., Yang, Y.N., Liu, Y., Tang, G.Q., 2013. Monazite and xenotime U-Th–Pb geochronology by ion microprobe: dating highly fractionated granites at Xihuashan tungsten mine, SE China. Contrib. Miner. Petr. 166, 65–80.
Li, X.F., Cheng, H., Wang, C.Z., Wang, L.F., 2016. Genesis of the Huangshaping W-Mo–Cu–Pb–Zn polymetallic deposit in Southeastern Hunan Province, China: constraints from fluid inclusions, trace elements, and isotopes. Ore Geol. Rev. 79, 1–25.
Li, X.H., Li, W.X., Wang, X.C., Li, Q.L., Liu, Y., Tang, G.Q., 2009. Role of mantle-derived magma in genesis of early Yanshanian granites in the Nanling Range, South China: in situ zircon Hf-O isotopic constraints. Sci. China Se.r D- Earth Sci. 52, 1262–1278.
Li, Z.L., Hu, R.Z., Yang, J.S., Peng, J.T., Li, X.M., Bi, X.W., 2007. He, Pb and S isotopic constraints on the relationship between the A-type Qitianling granite and the Furong tin deposit, Hunan Province, China. Lithos 97, 161–173.
Liu, J.Q., Wang, X.W., Zeng, Y.S., Wang, X.D., 2002. The Xihuashan granite and evolution of ore-forming fluid of tungsten-tin-beryllium ore field. Geol. Miner. Res. South China 3, 91–96 (in Chinese with English abstract).
Liu, Q., Yu, J.H., O'Reilly, S.Y., Zhou, M.F., Griffin, W.L., Wang, L., Cui, X., 2014. Origin and geological significance of Paleoproterozoic granites in the northeastern Cathaysia Block, South China. Precambr. Res. 248, 72–95.
Lu, H.Z., 1986. In: The Origin of Tungsten Mineral Deposits in South China. Chongqing Publishing House, Chongqing, pp. 1–232 (in Chinese).
Lü, K., Wang, Y., Xiao, J., 2011. Geochemistry characteristics of Xihuashan granite and structural environment discussion. J. East China Inst. Technol. 34, 117–128 (in Chinese with English abstract).
Lupton, J.E., Baker, E.T., Massoth, G.J., 1989. Variable ^{3}He/heat ratios in submarine hydrothermal systems: evidence from two plumes over the Juan de Fuca ridge. Nature 337, 161–164.
Mao, J.W., Cheng, Y.B., Chen, M.H., Pirajno, F., 2013a. Major types and time-space distribution of Mesozoic ore deposits in South China and their geodynamic settings. Miner. Depos. 48, 267–294.
Mao, J.W., Xie, G.Q., Guo, C.L., Chen, Y.C., 2007. Large-scale tungsten-tin mineralization in the Nanling region, South China: metallogenic ages and corresponding geodynamic processes. Acta Petrol. Sin. 23, 2329–2338 (in Chinese with English abstract).
Mao, J.W., Xie, G.Q., Guo, C.L., Yuan, S.D., Cheng, Y.B., Chen, Y.C., 2008. Spatial-temporal distribution of Mesozoic ore deposits in South China and their metallogenic settings. Geol. J. Chin. Univ. 14, 510–526 (in Chinese with English abstract).
Mao, J.W., Xiong, B.K., Liu, J., Pirajno, F., Cheng, Y.B., Ye, H.S., Song, S.W., Dai, P., 2017. Molybdenite Re/Os dating, zircon U-Pb age and geochemistry of granitoids in the Yangchuling porphyry W–Mo deposit (Jiangnan tungsten ore belt), China: implications for petrogenesis, mineralization and geodynamic setting. Lithos 286–287, 35–52.
Mao, Z.H., Cheng, Y.B., Liu, J.J., Yuan, S.D., Wu, S.H., Xiang, X.K., Luo, X.H., 2013b. Geology and molybdenite Re–Os age of the Dahutang granite-related veinlets-disseminated tungsten ore field in the Jiangxin Province, China. Ore Geol. Rev. 53, 422–433.
Mao, Z.H., Liu, J.J., Mao, J.W., Deng, J., Zhang, F., Meng, X.Y., Xiong, B.K., Xiang, X.K., Luo, X.H., 2015. Geochronology and geochemistry of granitoids related to the giant Dahutang tungsten deposit, middle Yangtze River region, China: implications for petrogenesis, geodynamic setting, and mineralization. Gondwana Res. 28, 816–836.
Marschik, R., Kendrick, M.A., 2015. Noble gas and halogen constraints on fluid sources in iron oxide-copper-gold mineralization: Mantoverde and La Candelaria, Northern Chile. Miner. Depos. 50, 357–371.
McKee, E.H., Rytuba, J.J., Xu, K.Q., Giuliani, G., 1987. Geochronology of the Xihuashan composite granitic body and tungsten mineralization, Jiangxi Province, South China. Econ. Geol. 82, 218–223.
Moura, A., Dória, A., Neiva, A.M.R., Leal Gomes, C., Creaser, R.A., 2014. Metallogenesis at the Carris W-Mo–Sn deposit (Gerês, Portugal): constraints from fluid inclusions, mineral geochemistry, Re–Os and He–Ar isotopes. Ore Geol. Rev. 56, 73–93.
Mu, Z.G., Huang, F.S., Chen, C.Y., Zheng, S.H., Fan, S.L., Liu, D.R., Mei, Y.W., 1981. Oxygen, hydrogen and carbon isotope studies of Piaotang and Xihuashan quartz vein-type tungsten deposits, Jiangxi Province. In: Proceedings of Symposium on Tungsten Geology. Geological Publishing House, Beijing, pp. 153–169 (in Chinese).
Oxburgh, E., O'nions, R., Hill, R., 1986. Helium isotopes in sedimentary basins. Nature 324, 632–635.
Shen, W.Z., Xu, S.J., Wang, Y.X., Yang, J.D., 1994. Study on the Nd–Sr isotope of the Xihuashan granite. China Sci. Bull. 39, 154–156 (in Chinese).
Simmons, S.F., Sawkins, F.J., Schlutter, D.J., 1987. Mantle-derived helium in two Peruvian hydrothermal ore deposits. Nature 329, 429–432.
Stuart, F.M., Burnard, P.G., Taylor, R.P., Turner, G., 1995. Resolving mantle and crustal contributions to ancient hydrothermal fluids: He-Ar isotopes in fluid inclusions from Dae Hwa W-Mo mineralisation, South Korea. Geochim. Cosmochim. Acta 59, 4663–4673.
Stuart, F.M., Turner, G., Duckworth, R.C., Fallick, A.E., 1994. Helium isotopes as tracers of trapped hydrothermal fluids in ocean-floor sulfides. Geology 22, 823–826.
Tanelli, G., 1982. Geological setting, mineralogy and genesis of tungsten mineralization in Dayu district, Jiangxi (People's Republic of China): an outline. Miner. Depos. 17, 279–294.
Turner, G., Burnard, P., Ford, J.L., Gilmour, J.D., Lyon, I.C., Stuart, F.M., 1993. Tracing fluid sources and interactions. Philos. Trans. – Royal Soc. London, Phys. Sci. Eng. 344, 127–140.
Wang, F.Y., Li, C.Y., Ling, M.X., Zhang, H., Sun, Y.L., Sun, W.D., 2011. Geochronology of the Xihuashan tungsten eeposit in Southeastern China: constraints from Re–Os and U-Pb dating. Res. Geol. 61, 414–423.
Wang, X.L., Zhou, J.C., Wan, Y.S., Kitajima, K., Wang, D., Bonamici, C., Qiu, J.S., Sun, T., 2013. Magmatic evolution and crustal recycling for Neoproterozoic strongly peraluminous granitoids from southern China: Hf and O isotopes in zircon. Earth Planet. Sci. Lett. 366, 71–82.
Wang, X.D., Ni, P., Jiang, S.Y., Zhao, K.D., Wang, T.G., 2010. Origin of ore-forming fluid in the Piaotang tungsten deposit in Jiangxi Province: evidence from helium and argon isotopes. China Sci. Bull. 55, 628–634.
Wang, Y., 2008. Some further discussion on the granitic types of the Early Yanshanian (Jurassic) granitoids in the Nanling area, SE China. Geol. Rev. 54, 162–174 (in Chinese with English abstract).
Wei, W.F., Hu, R.Z., Bi, X.W., Peng, J.T., Su, W.C., Song, S.Q., Shi, S.H., 2012. Infrared microthermometric and stable isotopic study of fluid inclusions in wolframite at the Xihuashan tungsten deposit, Jiangxi province, China. Miner. Depos. 47, 589–605.
Wei, W.F., Shen, N.P., Yan, B., Lai, C.K., Yang, J.H., Gao, W., Liang, F., 2018. Petrogenesis of ore-forming granites with implications for W-mineralization in the super-large Shimensi tungsten-dominated polymetallic deposit in northern Jiangxi Province, South China. Ore Geol. Rev. 95, 1123–1139.
Wei, W.F., Yan, B., Shen, N.P., Liu, L., Zhang, Y., Xiang, X.K., 2017. Muscovite ^{40}Ar/^{39}Ar age and H-O–S isotopes of the Shimensi tungsten deposit (northern Jiangxi Province, South China) and their metallogenic implications. Minerals 7, 1–15.
Wu, L.Y., Hu, R.Z., Peng, J.T., Bi, X.W., Jiang, G.H., Chen, H.W., Wang, Q.Y., Liu, Y.Y., 2011. He and Ar isotopic compositions and genetic implications for the giant Shizhuyuan W-Sn-Bi-Mo deposit, Hunan Province, South China. Int. Geol. Rev. 53, 677–690.
Wu, Y.L., Mei, Y.W., Liu, P.C., Cai, C.L., Lu, T.Y., 1987. In: Geology of the Xihuashan Tungsten Ore Field. Geological Publishing House, Beijing, pp. 1–317 (in Chinese).
Xiao, J., Wang, Y., Hong, Y.L., Zhou, Y.Z., Xie, M.H., Wang, D.S., Guo, J.S., 2009. Geochemistry characteristics of Xihuashan tungsten granite and its relationship to tungsten metallogenesis. J. East Chin. Inst. Technol. 32, 22–31 (in Chinese with English abstrat).
Xie, G.Q., Mao, J.W., Bagas, L., Fu, B., Zhang, Z.Y., 2018a. Mineralogy and titanite geochronology of the Caojiaba W deposit, Xiangzhong metallogenic province, southern China: implications for a distal reduced skarn W formation. Miner. Depos. https://doi.org/10.1007/s00126-018-0816-2.
Xie, G.Q., Mao, J.W., Li, W., Fu, B., Zhang, Z.Y., 2018b. Granite-related Yangjiashan tungsten deposit, southern China. Miner. Depos. https://doi.org/10.1007/s00126-018-0805-5.
Xie, G.Q., Mao, J.W., Li, W., Zhu, Q.Q., Liu, H.B., Jia, G.H., Li, Y.H., Li, J.J., Zhang, J., 2016. Different proportion of mantle-derived noble gases in the Cu–Fe and Fe skarn deposits: He–Ar isotopic constraint in the Edong district, Eastern China. Ore Geol. Rev. 72, 343–354.
Xu, L., Bi, X.W., Hu, R.Z., Tang, Y., Jiang, G., Qi, Y., 2014. Origin of the ore-forming fluids of the Tongchang porphyry Cu–Mo deposit in the Jinshajiang-Red River alkaline igneous belt, SW China: constraints from He, Ar and S isotopes. J. Asian Earth Sci. 79, 884–894.
Xu, X., O'Reilly, S.Y., Griffin, W.L., Wang, X., Pearson, N.J., He, Z., 2007. The crust of Cathaysia: age, assembly and reworking of two terranes. Precambr. Res. 158, 51–78.
Yan, D.P., Zhou, M.F., Song, H.L., Wang, X.W., Malpas, J., 2003. Origin and tectonic significance of a Mesozoic multi-layer over-thrust system within the Yangtze Block (South China). Tectonophysics 361, 239–254.
Yang, J.H., Kang, L.F., Peng, J.T., Zhong, H., Gao, J.F., Liu, L., 2018. In-situ elemental and isotopic compositions of apatite and zircon from the Shuikoushan and Xihuashan granitic plutons: implication for Jurassic granitoid-related Cu–Pb–Zn and W mineralization in the Nanling Range, South China. Ore Geol. Rev. 93, 382–403.
Yang, J.H., Peng, J.T., Zhao, J.H., Fu, Y.Z., Yang, C., Hong, Y.L., 2012. Petrogenesis of the Xihuashan granite in Southern Jiangxi Province, South China: constraints from zircon U-Pb geochronology, geochemistry and Nd isotopes. Acta Geosci. Sin. 86, 131–152.
Yao, J.L., Shu, L.S., Santosh, M., 2011. Detrital zircon U-Pb geochronology, Hf-isotopes and geochemistry-New clues for the Precambrian crustal evolution of Cathaysia Block, South China. Gondwana Res. 20, 553–567.
Yu, J.H., O'Reilly, S.Y., Wang, L.J., Griffin, W.L., Zhou, M.F., Zhang, M., Shu, L.S., 2010. Components and episodic growth of Precambrian crust in the Cathaysia Block, South China: evidence from U-Pb ages and Hf isotopes of zircons in Neoproterozoic sediments. Precambr. Res. 181, 97–114.
Yu, Y., Xu, X.S., Griffin, W.L., O'Reilly, S.Y., Xia, Q.K., 2011. H_2O contents and their modification in the Cenozoic subcontinental lithospheric mantle beneath the Cathaysia block, SE China. Lithos 126, 182–197.
Yuan, S.D., Mao, J.W., Nigel, J.C., Wang, X.D., Liu, X.F., Yuan, Y.B., 2015. A Late Cretaceous tin metallogenic event in Nanling W-Sn metallogenic province: constraints from U–Pb, Ar–Ar geochronology at the Jiepailing Sn–Be–F deposit, Hunan, China. Ore Geol. Rev. 65, 283–293.
Yuan, S.D., Williams-Jones, A.E., Mao, J.W., Zhao, P.L., Yan, C., Zhang, D.L., 2018a. The origin of the Zhangjialong tungsten deposit, South China: implications for W-Sn mineralization in large granite batholiths. Econ. Geol. 113, 1193–1208.
Yuan, S.D., Zhang, D.L., Shuang, Y., Du, A.D., Qu, W.J., 2012. Re–Os dating of molybdenite from the Xintianling giant tungsten-molybdenite deposit in southern Hunan Province, China and its geological implications. Acta Petrol. Sin. 28, 27–38.
Yuan, Y.B., Yuan, S.D., Mao, J.W., Zhao, P.L., Yan, C., Zhao, H.J., Zhang, D.L., Shuang, Y., Peng, J.T., 2018b. Recognition of Late Jurassic W-Sn mineralization and its exploration potential on the western margin of the Caledonian Guidong granite batholith, Nanling Range, South China: geochronological evidence from the Liuyuan Sn and Zhuyuanli W deposits. Ore Geol. Rev. 93, 200–210.
Zeng, Y.S., Zhu, Y.F., Liu, J.Q., 2001. Carbonaceous material in S-type Xihuashan granite. Geochem. J. 35, 145–154.
Zhai, W., Sun, X.M., Wu, Y.S., Sun, Y.Y., Hua, R.M., Ye, X.R., 2012. He-Ar isotope geochemistry of the Yaoling-Meiziwo tungsten deposit, North Guangdong Province:

constraints on Yanshanian crust-mantle interaction and metallogenesis in SE China. China Sci. Bull. 57, 1150–1159.
Zhang, D.L., Zheng, D.S., Peng, J.T., Yuan, S.D., 2011. A preliminary study of the retention of noble gases in fluid inclusions of different minerals. Min. Depos. 30, 933–940 (in Chinese with English abstract).
Zhang, L.G., Zhuang, L.C., Qian, Y.Q., Guo, Y.S., Zhai, P., 1981. Stable isotope geochemistry of granites and tungsten-tin deposits in Xihuashan-Piaotang area, Jiangxi Province, China. In: Proceedings of Symposium on Tungsten Geology. Geological Publishing House, Beijing, pp. 325–338 (in Chinese).
Zhang, Q., Zhang, R.Q., Gao, J.F., Lu, J.J., Wu, J.W., 2018. In-situ LA-ICP-MS trace element analyses of scheelite and wolframite: constraints on the genesis of veinlet-disseminated and vein-type tungsten deposits, South China. Ore Geol. Rev. 99, 166–179.
Zhao, J.H., Zhou, M.F., Yan, D.P., Zheng, J.P., Li, J.W., 2011. Reappraisal of the ages of Neoproterozoic strata in South China: no connection with the Grenvillian orogeny. Geology 39, 299–302.
Zhao, P.L., Yuan, S.D., Mao, J.W., Santosh, M., Li, C., Hou, K.J., 2016. Geochronological and petrogeochemical constraints on the skarn deposits in Tongshanling ore district, southern Hunan Province: implications for Jurassic Cu and W metallogenic events in South China. Ore Geol. Rev. 78, 120–137.
Zhao, P.L., Yuan, S.D., Mao, J.W., Yuan, Y.B., Zhao, H.J., Zhang, D.L., Shuang, Y., 2018. Constraints on the timing and genetic link of the large-scale accumulation of proximal W-Sn–Mo–Bi and distal Pb–Zn–Ag mineralization of the world-class Dongpo orefield, Nanling range, South China. Ore Geol. Rev. 95, 140–1160.
Zheng, J., O'Reilly, S.Y., Griffin, W.L., Zhang, M., Lu, F., Liu, G., 2004. Nature and evolution of Mesozoic-Cenozoic lithospheric mantle beneath the Cathaysia block, SE China. Lithos 74, 41–65.
Zhong, J., Chen, Y.J., Pirajno, F., 2017. Geology, geochemistry and tectonic settings of the molybdenum deposits in South China: a review. Ore Geol. Rev. 81, 829–855.
Zhou, M.F., Ma, Y.X., Yan, D.P., Xia, X.P., Zhao, J.H., Sun, M., 2006. The Yanbian terrane (Southern Sichuan Province, SW China): a Neoproterozoic arc assemblage in the western margin of the Yangtze Block. Precambr. Res. 144, 19–38.
Zhou, M.F., Yan, D.P., Kennedy, A.K., Li, Y.Q., Ding, J., 2002. SHRIMP U-Pb zircon geochronological and geochemical evidence for Neoproterozoic arc-magmatism along the western margin of the Yangtze Block, South China. Earth Planet. Sci. Lett. 196, 51–67.
Zhou, Y.Z., Gao, C.S., Hong, Y.L., Han, Z.X., Wen, L.H., 2010. Diagenesis-mineralization process and mineralization models of Xihuashan granite. China Tungsten Industry 25, 12–16 (in Chinese with English abstract).
Zhu, J.C., Wang, R.C., Zhang, P.H., Xie, C.F., Zhang, W.L., Zhao, K.D., 2009. Zircon U-Pb geochronological framework of Qitianling granitic batholith, middle part of Nanling Range, South China. Sci. China Earth Sci. 39, 1112–1127 (in Chinese with English abstract).